INL/CON-16-39170
PREPRINT

MODELING AND ANALYSIS OF FISSION PRODUCT TRANSPORT IN THE AGR-3/4 EXPERIMENT

2016 International Topical Meeting on High Temperature Reactor Technology (HTR 2016)

Paul W. Humrickhouse, Blaise P. Collin,
Grant L. Hawkes, Jason M. Harp,
Paul A. Demkowicz, David A. Petti

November 2016

The INL is a
U.S. Department of Energy
National Laboratory
operated by
Battelle Energy Alliance

MODELING AND ANALYSIS OF FISSION PRODUCT TRANSPORT IN THE AGR-3/4 EXPERIMENT

Paul W. Humrickhouse, Blaise P. Collin, Grant L. Hawkes, Jason M. Harp, Paul A. Demkowicz, and David A. Petti

Idaho National Laboratory: PO box 1625, Idaho Falls, ID, 83415, paul.humrickhouse@inl.gov

In this work we describe the ongoing modeling and analysis efforts in support of the AGR-3/4 experiment. AGR-3/4 is intended to provide data to assess fission product retention and transport (e.g., diffusion coefficients) in fuel matrix and graphite materials. We describe a set of pre-test predictions that incorporate the results of detailed thermal and fission product release models into a coupled 1D radial diffusion model of the experiment, using diffusion coefficients reported in the literature for Ag, Cs, and Sr. We make some comparisons of the predicted Cs profiles to preliminary measured data and find these to be reasonable, in most cases within an order of magnitude. Our ultimate objective is to refine the diffusion coefficients using AGR-3/4 data, so we develop an analytical method for doing so and demonstrate its efficacy via a series of numerical experiments using the model predictions.

I. INTRODUCTION

One of the primary goals of the Advanced Gas Reactor (AGR) Fuel Development and Qualification Program is to provide a fuel qualification data set in support of the licensing of a modular HTGR.[1] AGR-3/4 combines the third and fourth installments of a series of fuel irradiation experiments undertaken in support of that goal. In contrast to the fuel "shakedown" and performance tests (AGR-1 and AGR-2, respectively), which successfully demonstrated the performance of the tristructural-isotropic (TRISO) fuel itself, the purpose of AGR-3/4 is to provide data on fission product sorptivities and diffusivities in compact matrix and graphite materials for use in revising fission product transport models.

The primary purpose of this work is to describe these existing fission product transport models, and how they are being used to support planning for post-irradiation examination (PIE) and analysis of AGR-3/4. We describe the pre-test predictions made with the model, and are now able to make some preliminary comparisons with data, measured via gamma-scanning.[2] Making use of the data obtained from AGR-3/4, however, requires solving the inverse problem- determining diffusion coefficients from measured profiles, rather than predicting profiles based on given diffusivities. This is a non-trivial exercise as a result of the many coupled transport phenomena that combine to produce the profiles that we ultimately measure in AGR-3/4. We discuss our approach for obtaining diffusivities from measured concentration profiles, and explore some analytical techniques that appear suitable for the analysis despite these complexities. We use the model to conduct a series of numerical experiments to demonstrate feasibility, and apply it to estimate the diffusivity of europium in matrix based on the preliminary experiment data.

II. AGR-3/4 EXPERIMENT OVERVIEW

The AGR-3/4 experiment is described in detail elsewhere,[3-5] but we outline some of the salient details here. The AGR-3/4 test train consisted of 12 capsules stacked vertically (Fig. 1), irradiated for ~370 effective full power days (to 5-15% FIMA) from 2011-2014 in the northeast flux trap of the Advanced Test Reactor (ATR). Each capsule contains at its center a fuel stack consisting of four cylindrical compacts, 12.3 mm in diameter and each 12.5 mm high. The compacts are composed of a matrix material in which are embedded TRISO-coated driver fuel particles with UCO kernels, ~1872 per compact, plus an additional 20 designed-to-fail (DTF) particles. These DTF particles were aligned vertically along the axial centerline of the compacts. They possessed only a kernel and a 20 μm thick highly anisotropic pyrolytic carbon coating (i.e. no SiC) such that they could be expected to fail early in the irradiation and thereby provide a relatively constant source of fission products at the centerline of the capsule.

These fission products are then expected to transport radially outward across a series of concentric rings, as illustrated in Fig 2. The fuel stack is followed by the inner ring (IR), typically (though not always) matrix, followed by the graphite (PCEA or IG-110) outer ring (OR), and finally by the sink ring (also graphite), so named because it is sufficiently cold to trap fission products that reach it. The inner and outer rings have nominal outer diameters of 24.4 and 39.0 mm, respectively, and while the heights differ slightly depending on the capsule type (there are "fuel body" and

"standard" types which serve different purposes in PIE), the standard height is 50.8 mm.

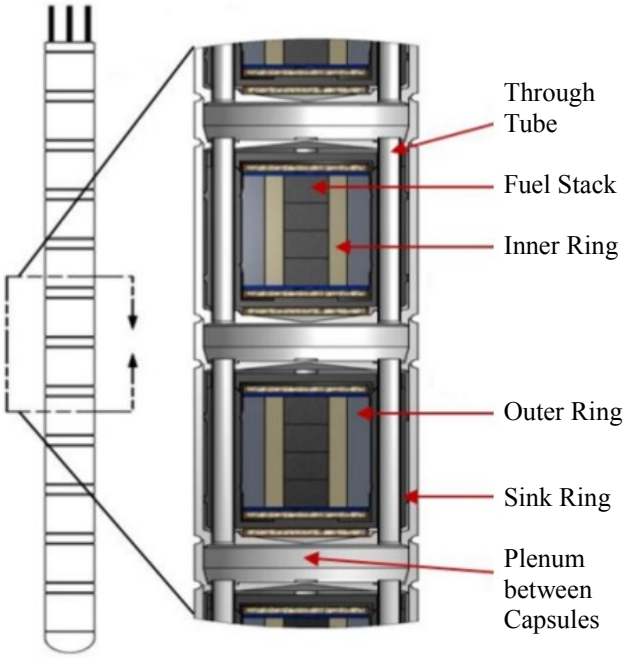

Fig. 1. Schematic of the AGR-3/4 test train.

Temperatures were controlled independently in each capsule by adjusting the composition of a mixture of helium and neon gases, which serves additionally to sweep gaseous fission products from the capsule, and these were measured during the course of the experiment. Altering the gas composition allows for temperature control by changing the conductivity of the gas in the gaps between the rings (100% helium for high conductivity and 100% neon for low conductivity). This gas flows primarily through gaps on either side of the sink ring, though it also fills smaller gaps in between the compacts and inner ring, and inner and outer rings. The gas mixture was adjusted during the course of the experiment to maintain the desired peak fuel temperature (in capsules 1, 3, 6, 7, 11, and 12) or inner/outer ring temperature (in capsules 2, 4, 5, 8, 9, and 10). The result is a reasonably constant temperature across each ring, though these do vary in time as the power, gas composition, and gap widths change. The predicted[6] time-averaged volume-averaged (TAVA) temperatures for the rings are summarized in Table I.

III. MODEL DESCRIPTION

The model assumes that fission products diffuse radially through each cylindrical ring:

$$\frac{\partial C(r,t)}{\partial t} = \frac{1}{r}\frac{\partial}{\partial r}\left(rD\frac{\partial C(r,t)}{\partial r}\right) \qquad (1)$$

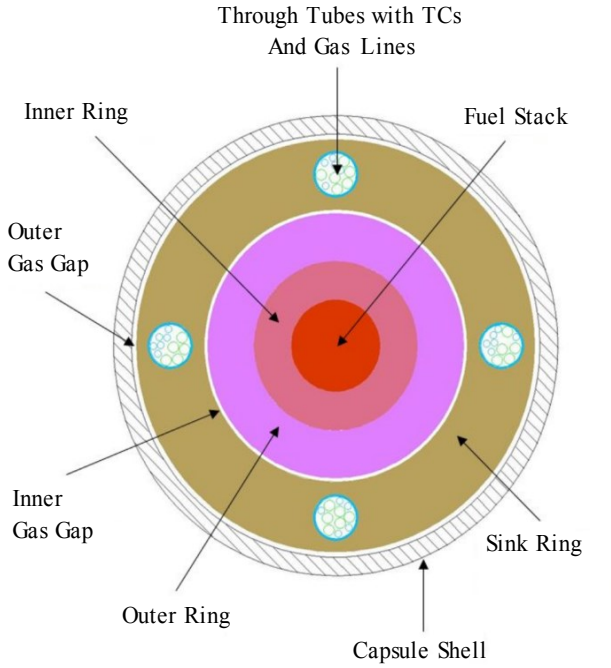

Fig. 2. Arrangement of concentric rings in an AGR-3/4 capsule.

TABLE I. Summary of time-averaged volume-averaged (TAVA) temperatures in AGR-3/4.[6]

	Inner Ring		Outer Ring	
Capsule	Material	TAVA	Material	TAVA
1	Matrix	853 °C	PCEA	765 °C
2	Matrix	934 °C	PCEA	859 °C
3	PCEA	1026 °C	PCEA	962 °C
4	Matrix	820 °C	PCEA	708 °C
5	Matrix	800 °C	PCEA	677 °C
6	Matrix	843 °C	PCEA	707 °C
7	Matrix	1151 °C	PCEA	1025 °C
8	IG-110	1021 °C	IG-110	917 °C
9	Matrix	822 °C	IG-110	698 °C
10	PCEA	1038 °C	PCEA	971 °C
11	Matrix	1124 °C	PCEA	966 °C
12	Matrix	782 °C	PCEA	741 °C

We consider diffusion only in the radial direction, and the concentric ring configuration of the experiment was intended to provide as close to a 1D approximation as possible, although it is not precisely so due to the presence of some axial temperature gradients.

While a 1D diffusion model in principle provides simple ways to estimate diffusion coefficients from the experiment data, in practice, due to the semi-integral

nature of the AGR-3/4 experiment, it is complicated by a number of factors.

First is the presence of gaps between the rings. In this configuration, rather than a continuous concentration across the ring interface, fission products must first desorb into a vapor phase in the gap, and subsequently adsorb on the next ring before diffusing into it. We model these processes with established sorption isotherm models, but these introduce a number of additional material parameters that are themselves uncertain, or unknown depending on the fission product of interest.

Both the diffusion coefficients and sorption isotherms are temperature dependent, and so there is a need for an accompanying thermal model. Temperatures do change over the course of the irradiation, complicating the notion of a single "temperature" associated with a given fission product profile. Because a detailed thermal model of the experiment was developed as a part of standard ATR pre- and post-experiment analyses, we use its results as input here.

Finally, it is necessary to define a source term. Though the DTF particles were intended to provide a known source of fission products, in practice they may not lose all of their fission products, may not all fail at time zero[5] (as was assumed in the modeling), and there may be additional contributions to the total release from a much larger number of intact particles (e.g., Ag).

To address these additional complexities, we have relied on a suite of modeling tools. Physics calculations[7] provide heat rates and fission product inventories. From the heat rates, material conductivities, and sweep gas measurements, temperatures are calculated.[8] PARFUME is used to calculate the fission product release source, *S(t)*, from intact and the DTF particles.[9] This information along with diffusion coefficient data for fission products in matrix and graphite are used to calculate the concentration profiles in the different rings. The flow of information between these codes is illustrated in Fig. 3, and a summary of the computations performed with each is given below.

III.A. Thermal Analysis

The thermal analysis was performed[6,8] with a detailed 3D model in ABAQUS; a schematic and representative mesh are shown in Fig. 4. A steady-state temperature distribution was solved for each day of irradiation, based on nuclear heating from the as-run physics analysis with MCNP. The variation of thermal conductivity of graphite and matrix with both temperature and fluence were accounted for, as was the changing gap conductivity. Both radiation and conduction were modeled in these gaps (advection was shown to be comparatively insignificant), as was the change over time of the gap conductivity based on changes in both gas composition (helium/neon mixture) and the gap width. The latter was due to dimensional changes of the rings occurring as a result of neutron damage during irradiation, and the model was updated to reflect the actual dimensional changes that have now been measured in PIE.

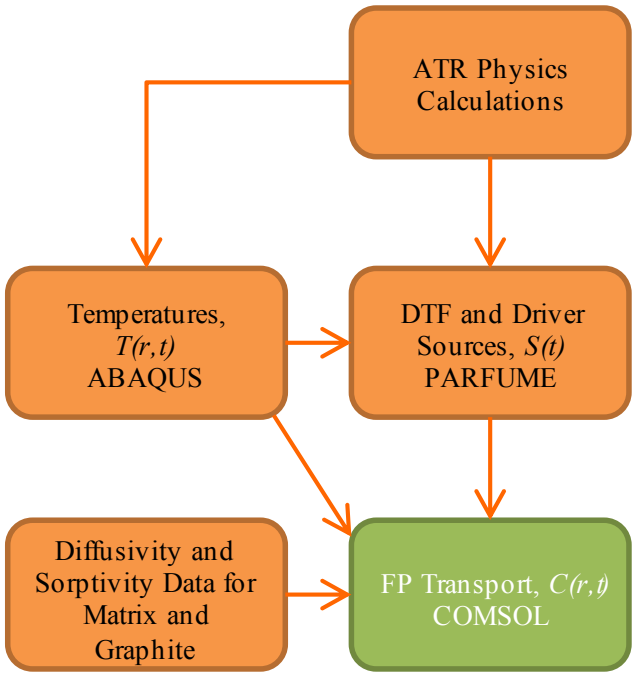

Fig. 3. Codes used to inform this work, and the flow of information between them.

The gap conductivity model described in Refs. 6 and 8 was adjusted so as to give temperature predictions that more closely matched the values measured over the course of the irradiation. Temperatures were relatively constant over the first four cycles of irradiation, during which the model was accurate to within ~10 °C, but increased somewhat in the final three cycles as the gaps shrank and the temperature became more difficult to control. The model under predicts this increase by as much as 60 °C, though there is some uncertainty as to the accuracy of the thermocouple readings during this late stage of the irradiation. The temperature increase during this time has a significant impact on the source term, which is discussed in the next section.

Temperatures, as a function of time and radius, have been extracted along a radial line at the center (axially) of the capsule and provided as input to the COMSOL fission product transport analysis.

Source terms of Ag, Cs, and Sr in the COMSOL analysis are provided by PARFUME, which calculates the release of these fission products from the TRISO particle fuel; the calculations for AGR-3/4 are described in Ref. 9. Based on fission product inventories predicted by the as-run physics analysis and temperatures predicted by the

thermal analysis, PARFUME computes the probability of particle failure and resultant release, as well as the release from intact particles resulting from diffusion through the kernel, outer pyrolytic carbon, silicon carbide, and outer pyrolytic carbon layers in succession. No failures of the driver fuel particles were detected in the experiment[5] nor were any predicted by PARFUME; the source term therefore consists of the release from DTF and intact particles.

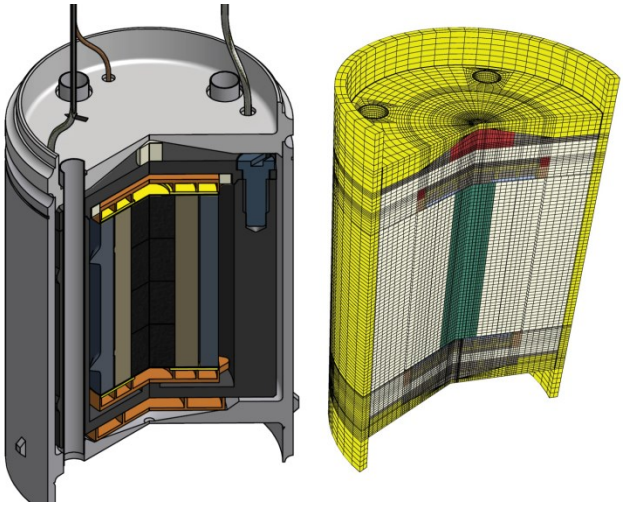

Fig. 4. Cutaway views of an AGR-3/4 capsule and corresponding ABAQUS mesh.

III.B. Fission Product Release from TRISO Particles

The predicted release fraction from DTF particles at the end of irradiation is near 100% for Ag and Cs in all capsules but 1 and 12 (the coldest), and ~2% in most cases for Sr, that coming from ejection by recoil (the diffusivity of Sr in kernels is thought to be low). While this DTF source was intended to be the primary one, release from intact particles was not always negligible, and since there are a factor of 100 more of them, this is in some cases comparable to or larger than the source from DTF particles. This is illustrated in Table II, where the relative contribution of DTF and driver sources is compared. Where the source comes primarily from DTF particles, it is highlighted in green; from driver fuel, in red. When both contribute comparably to the overall source they appear in yellow. The relative contribution also varies in time, most dramatically in capsule 7, the hottest in the experiment (Fig. 5). Here a relatively constant source of Cs from DTF particles is evident, but is eclipsed in magnitude by the driver source in later times, when a larger inventory exists in the fuel, and higher temperatures facilitate its release. We note that PARFUME models greatly over-predicted Cs releases in the AGR-1 experiment based on the historical database, and therefore should be regarded as a considerable source of uncertainty in this analysis.[10,11]

TABLE II. Primary contribution to the overall source term by fission product and capsule based on PARFUME predictions. Comparable means both the DTF and intact particles are contributing significantly to the source.

Capsule	Ag	Cs	Sr
1	DTF	DTF	DTF
2	Comparable	DTF	DTF
3	Driver	DTF	Comparable
4	Comparable	DTF	DTF
5	Comparable	DTF	DTF
6	Comparable	DTF	DTF
7	Driver	Comparable	Driver
8	Driver	DTF	Driver
9	Comparable	DTF	DTF
10	Driver	DTF	Driver
11	Driver	DTF	Driver
12	DTF	DTF	DTF

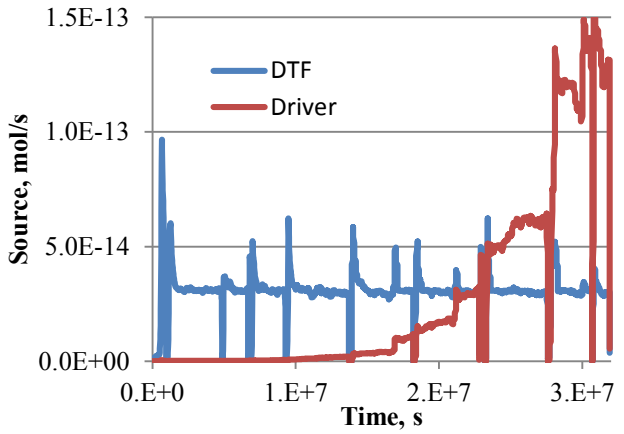

Fig. 5. PARFUME predicted release of Cs from DTF and driver particles in capsule 7. The abrupt drops and subsequent spikes are coincident with reactor shutdowns and corresponding temperature decreases and increases.

III.C. Fission Product Transport through Rings

The results of the ABAQUS and PARFUME analyses outlined above are used as inputs to the primary fission product transport calculation through the concentric rings, which is performed in COMSOL Multiphysics. This is a 1D calculation (Eq. 1) across four cylindrical regions representing the compact, inner ring, outer ring, and sink ring, respectively. PARFUME results for release of each fission product as a function of time for DTF and driver (intact) fuel are applied as volume sources in the compact; the DTF source is confined to a very narrow region near the axial centerline.

We use the same set of diffusion coefficients in the matrix and graphite for Ag, Cs, and Sr as used in Ref. 12, which are taken in turn from Refs. 13 and 14. These are given by the Arrhenius law,

$$D = D_0 \exp\left(-Q/RT\right) \qquad (2)$$

The parameters used for each isotope are listed in Table III, and the resultant diffusion coefficients are plotted over the range of interest in Fig. 6. Based on these we anticipate that silver will be the most mobile of the modeled fission products, followed by cesium (though note that this trend is reversed below ~1000 K, see Fig. 6), and then by the comparatively immobile strontium.

TABLE III. Diffusion coefficient Arrhenius parameters

Fission Product	Material	D_0 (m²/s)	Q (kJ/mol)
Ag	Matrix	1.6	258
	Graphite	1.38e-2	226
Cs	Matrix	3.60e-4	189
	Graphite	1.70e-6	149
Sr	Matrix	1.00e-2	303
	Graphite	1.70e-2	268

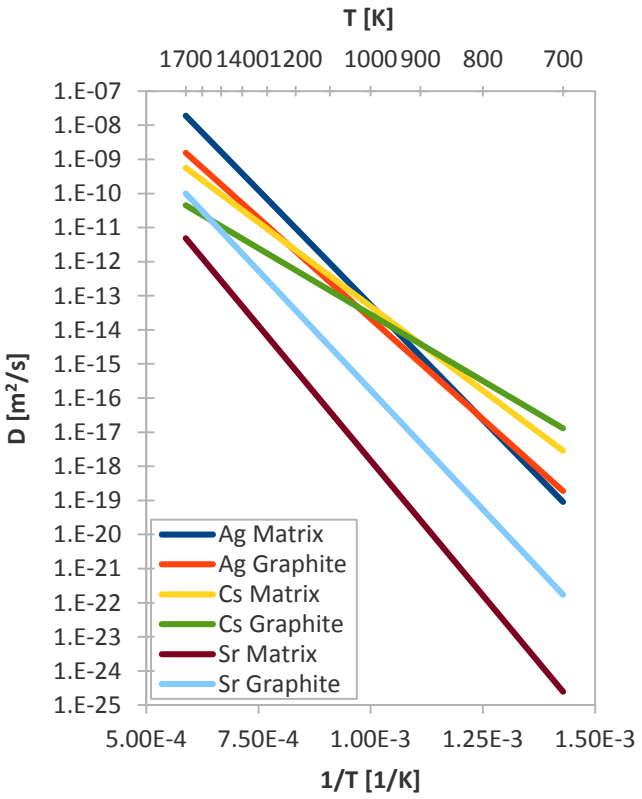

Fig. 6. Diffusion coefficients, as a function of temperature, used in this analysis.

Having defined the diffusion coefficients and source terms, we need finally to define the boundary conditions. These are given by established sorption isotherms,[12,14-15] which define an equilibrium relationship between the (volume) concentration of a given fission product near the surface of a solid, and its partial pressure above the surface. The relationship between the partial pressure P and the concentration C is thought to be linear at low concentrations (Henry's law), but transitions to a power law (Freundlich isotherm) above some threshold. Models encompassing both regimes have been obtained[12,15] by simply adding their contributions, viz.:

$$\frac{P}{P_{ref}} = \exp\left(A + \frac{B}{T}\right)\left(\frac{C}{C_{ref}}\right)^{\left(D+\frac{E}{T}\right)} + \exp\left[\left(A+\frac{B}{T}\right)+\left(D-1+\frac{E}{T}\right)\left(d_1 - d_2 T\right)\right]\frac{C}{C_{ref}} \qquad (3)$$

The parameters A, B, D, E, d_1, and d_2 are material constants that define the isotherms; here D is not to be confused with the diffusion coefficient. In writing the above, we have made explicit the use of a reference pressure and concentration. These have associated units, and tacit changes in the reference units (e.g. from Ref. 15 to Ref. 13) have resulted in different reported values of the parameter A, a point which has caused some confusion about its proper value.[16] The parameter values for cesium and strontium determined from experiments (and used in the model) are given in Table IV. In the absence of any experimentally-determined parameters for silver, our silver model simply employs the cesium isotherm parameters, the same approach adopted in Ref. 12.

TABLE IV. Sorption isotherm parameters.

	Cs		Sr	
	Matrix	Graphite	Matrix	Graphite
A [-]	19.3	24	54.3	19.4
B [K]	-47,300	-35,700	-149,000	-40,100
D [-]	1.51	-1.56	-8.52	-0.32
E [K]	4,340	6,120	28,500	4,090
d_1 [-]	3.4	2.04	3.13	-2.12
d_2 [1/K]	6.15e-4	1.79e-3	0	0
P_{ref}	1 [Pa]			
C_{ref}	1.77 [mol/m³]			

In AGR-3/4, because the temperatures (and usually the materials) differ at the ring edges on either side of each gap, the expected effect is a step change in concentration of a given fission product from the outside of one ring to the inside of the next. This is implemented in the model as a partition coefficient. If concentrations are sufficiently low to remain in the Henrian regime (and the models currently suggest they do, for all fission products in all capsules) then an explicit formula can be written for this partition coefficient from one surface (b) to the next (a):

$$\frac{C_b}{C_a} = \frac{\exp\left[\left(A_b + \frac{B_b}{T_b}\right) + \left(D_b - 1 + \frac{E_b}{T_b}\right)\left(d_{1,b} - d_{2,b}T_b\right)\right]}{\exp\left[\left(A_a + \frac{B_a}{T_a}\right) + \left(D_a - 1 + \frac{E_a}{T_a}\right)\left(d_{1,a} - d_{2,a}T_a\right)\right]} \quad (4)$$

If the materials are the same, the drop in temperature will result in an *increase* in concentration moving outward across the gap. Because the models suggest, for example, that graphite is less sorptive than matrix material for cesium, this change in properties can be more significant than the temperature decrease, and the concentration across a matrix/graphite ring interface drops. These behaviors are evident in Fig. 7, where some representative isotherms are plotted.

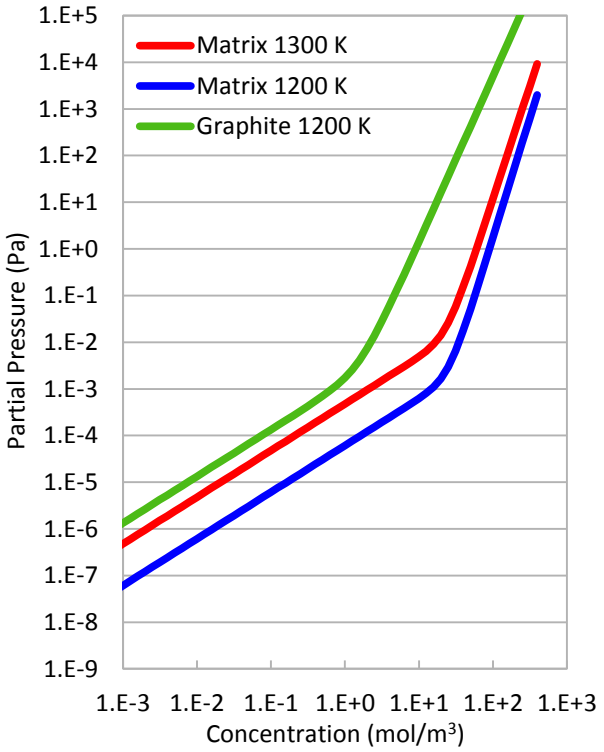

Fig. 7. Representative cesium sorption isotherms. Relative to matrix at 1300 K, matrix at 1200 K (and the same partial pressure) has a higher concentration; graphite at 1200 K has a lower concentration.

The end result of the fission product transport calculations are a set of concentration (e.g. in mol/m^3) profiles across the four regions (compact and inner, outer, and sink rings) for each fission product in each capsule. To better facilitate comparisons with measured data, we apply a few correction factors. First, because PARFUME computes release of all isotopes of a given element, and the COMSOL fission product transport calculations are based on these as source terms, we apply a correction factor based on the predicted end of life isotope ratios, which are computed independently for all compacts (four in each of 12 capsules). We take an average of the center two compacts for application to our 1D model, and these factors are given in Table V. Secondly, we convert mass to activity based on the decay constant for the isotopes of interest (^{110m}Ag, ^{134}Cs, ^{137}Cs, and ^{90}Sr). The final predicted profiles at the end of irradiation are depicted in Figs. 8-11. These represent our best estimates of the fission product concentration profiles in the AGR-3/4 experiment based on previously available diffusion coefficient and sorption isotherm parameters, and we make use of these results in approaching analysis of the AGR-3/4 data itself, and also in formulating a post-irradiation examination plan. We describe these activities in Sections V and VI below, respectively.

TABLE V. Correction factors for isotope fractions based on computed inventories and averaged over the two center compacts.

Capsule	$\frac{^{110m}\text{Ag}}{\text{Ag}}$	$\frac{^{134}\text{Cs}}{\text{Cs}}$	$\frac{^{137}\text{Cs}}{\text{Cs}}$	$\frac{^{90}\text{Sr}}{\text{Sr}}$
1	0.00263	0.01294	0.41172	0.56549
2	0.00481	0.02468	0.43292	0.56805
3	0.00637	0.03303	0.44219	0.56990
4	0.00746	0.03881	0.44717	0.57128
5	0.00802	0.04144	0.44905	0.57165
6	0.00827	0.04266	0.45000	0.57209
7	0.00815	0.04164	0.44949	0.57180
8	0.00779	0.03968	0.44828	0.57147
9	0.00712	0.03667	0.44565	0.57085
10	0.00591	0.03020	0.43959	0.56930
11	0.00427	0.02162	0.42831	0.56737
12	0.00225	0.01076	0.40578	0.56501

IV. COMPARISONS WITH MEASURED DATA

While a full post-irradiation examination of AGR-3/4 is planned but not yet executed, at this time we do have available results from tomographic gamma scans of selected rings, which are described in detail in a separate paper.[2] This allows for some preliminary comparisons of the model results to measured data.

Our first basis for comparison is the total activity in a given ring. Measured total activities obtained thus far are listed in Table VI along with their corresponding model predictions. The latter are obtained from the final model profile by simply integrating over the radius of the ring and multiplying by the ring height. In order to make a relative comparison of the two, the ratio of model to measured values is also shown.

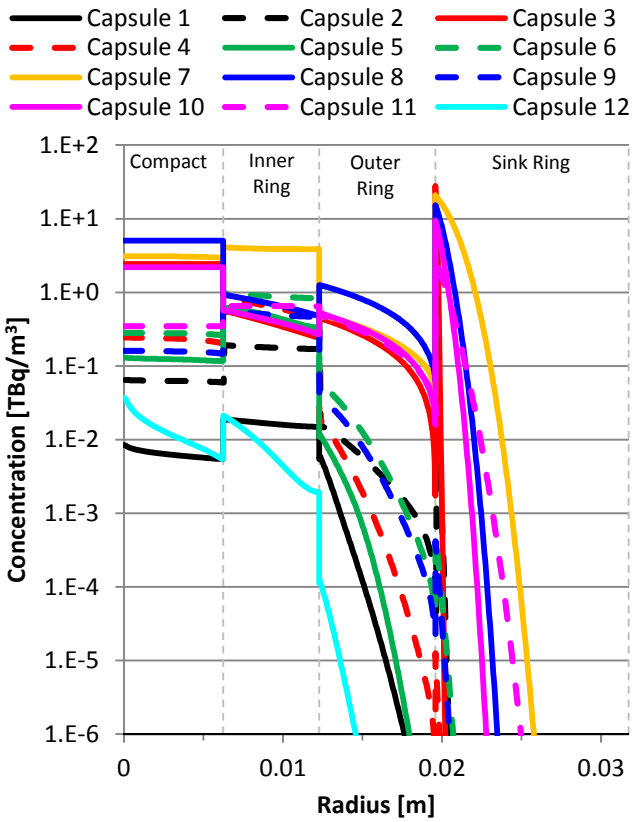

Fig. 8. Predicted ^{110m}Ag radial distributions in AGR-3/4.

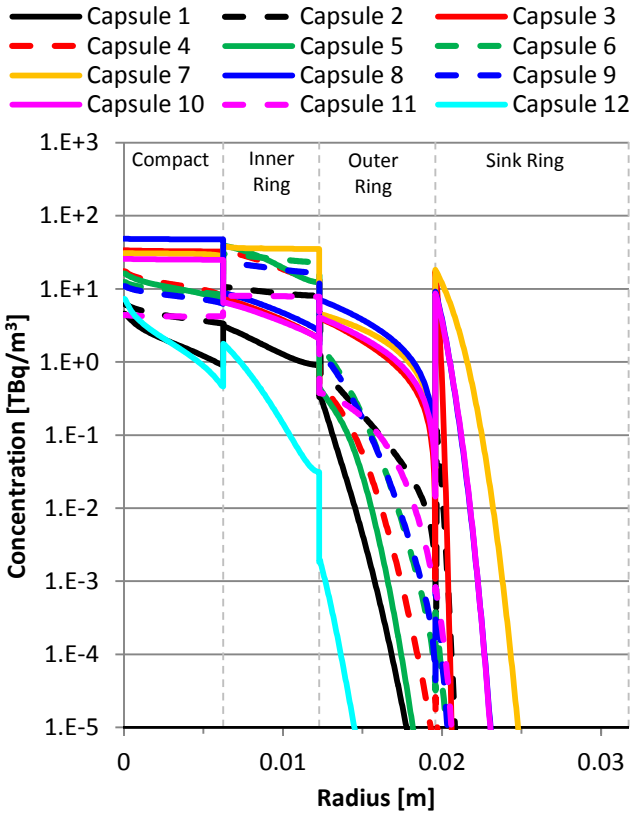

Fig. 9. Predicted ^{134}Cs radial distributions in AGR-3/4.

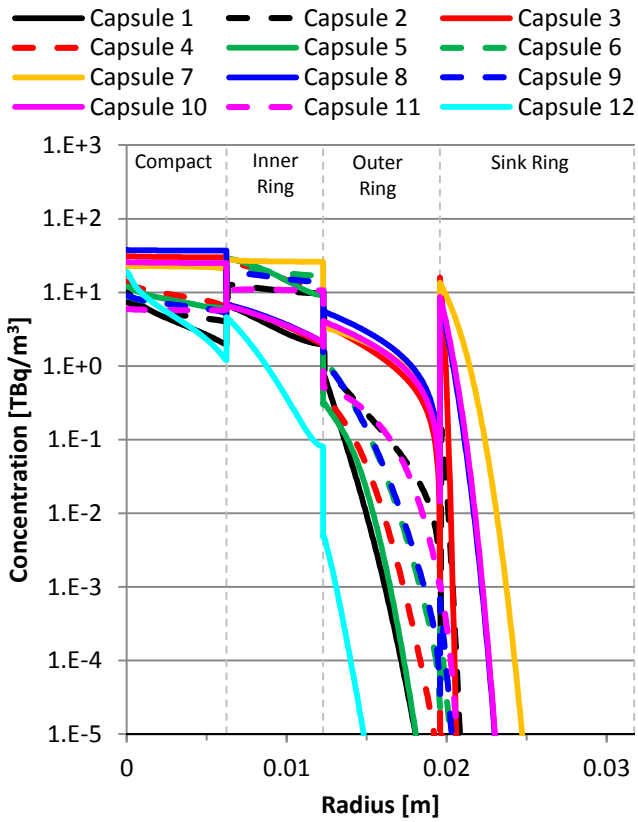

Fig. 10. Predicted ^{137}Cs radial distributions in AGR-3/4.

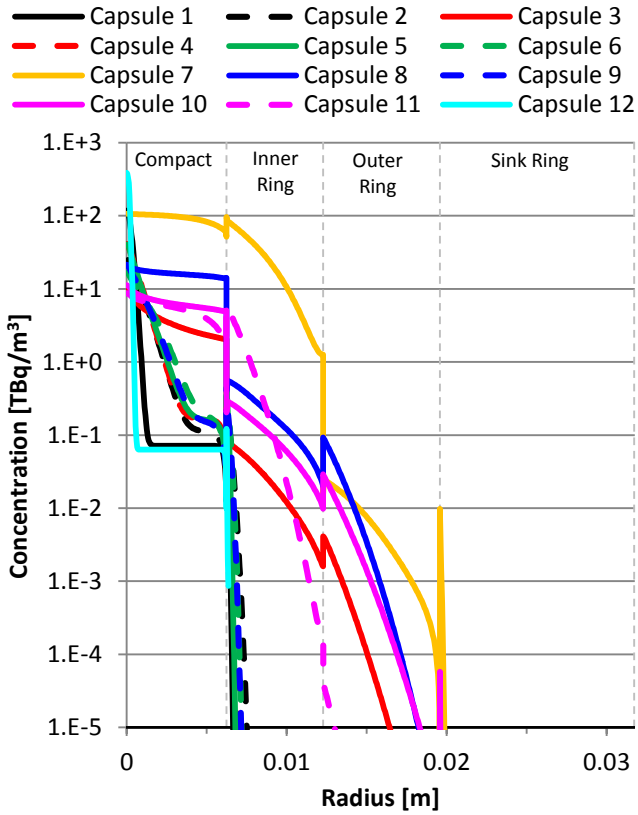

Fig. 11. Predicted ^{90}Sr radial distributions in AGR-3/4.

TABLE VI. Measured,[2] modeled (MBq), and the ratio of modeled to measured activity in selected rings.

	^{110m}Ag			^{134}Cs			^{137}Cs		
	Measured	Model	**Ratio**	Measured	Model	**Ratio**	Measured	Model	**Ratio**
IR-01	0.00	0.29	**N/A**	2.78	27.67	**9.97**	8.96	60.39	**6.74**
OR-01	0.00	0.02	**N/A**	0.10	0.97	**9.40**	1.25	2.13	**1.70**
IR-03	10.83	6.55	**0.60**	16.16	75.05	**4.64**	19.48	68.94	**3.54**
OR-03	38.81	7.17	**0.18**	13.57	54.18	**3.99**	14.94	49.77	**3.33**
OR-05	0.19	0.05	**0.27**	2.87	2.12	**0.74**	3.38	1.57	**0.47**
IR-07	0.13	69.39	**520.92**	24.85	633.13	**25.48**	21.84	469.01	**21.47**
OR-07	9.66	9.58	**0.99**	38.99	75.84	**1.95**	32.20	56.18	**1.74**
IR-08	32.70	11.97	**0.37**	26.55	92.84	**3.50**	26.98	71.97	**2.67**
OR-08	299.97	22.55	**0.08**	124.93	104.46	**0.84**	108.41	80.98	**0.75**
IR-10	20.71	7.10	**0.34**	19.74	69.64	**3.53**	23.83	69.55	**2.92**
OR-10	89.86	8.97	**0.10**	27.61	59.50	**2.16**	31.72	59.42	**1.87**

Table VI illustrates that even without any adjustment of the diffusion coefficients, the model presently does a reasonable job of estimating the measured inventories, and in most cases is within our acceptance criterion (+/- one order of magnitude). The inner ring (IR) of capsule 7 is a notable exception, and this is the hottest ring in the experiment. Silver activities tend to be under predicted, and the measured data exhibit other features that are contrary to the modeling approach, namely that there is a strong axial variation to the measured silver profile, peaked at the ends of the rings.[2] Such an observation makes a 1D (radial) approach to those data unsatisfactory, and an explanation for those observations is being sought as PIE continues.

Cesium, though, is a different matter. Tomographic scans of cesium activity permit a comparison of not just the total inventory, but also the radial profile across the ring. To do so, we must first convert the raw tomogram data, a relative intensity mapped on an *x*-*y* grid, to activity concentration. A direct calibration (by comparison with data obtained during destructive examination during PIE) is planned, but in the interim we can make an approximate estimation by assuming that the transformation is linear, and scaled to match the known integral activity.

We begin by simply converting the *x*-*y* values of the grid to r,θ values. The regular nature of the *x*-*y* grid results in a list of repeated r values, each at a different θ. We average each set of these values to obtain an azimuthally averaged intensity as a function of radius. This radial profile of arbitrary intensity values is then scaled such that its integral is equal to the measured integral activity from Table VI. At the time of this writing, intensity maps from three rings had been obtained: the inner rings of capsules 3, 7, and 10. Comparisons of the modeled and measured (at the axial center of the ring) cesium-137 radial distributions are shown in Figs. 12-14.

While the model predictions are not close for IR-07 (perhaps because the release from intact particles has been overestimated here), they are reasonable for both IR-03 and IR-10, in that they are within our established margin of +/- one order of magnitude, but are conservative (they overestimate the concentration), and have nearly the same slope toward the outer edge of the rings. It should be noted that some of the error in the model predictions may be due to an incorrect estimation of the source term (release from particles), which can be assessed when the inventories remaining in particles, compactsan overall mass balance is performed in PIE.

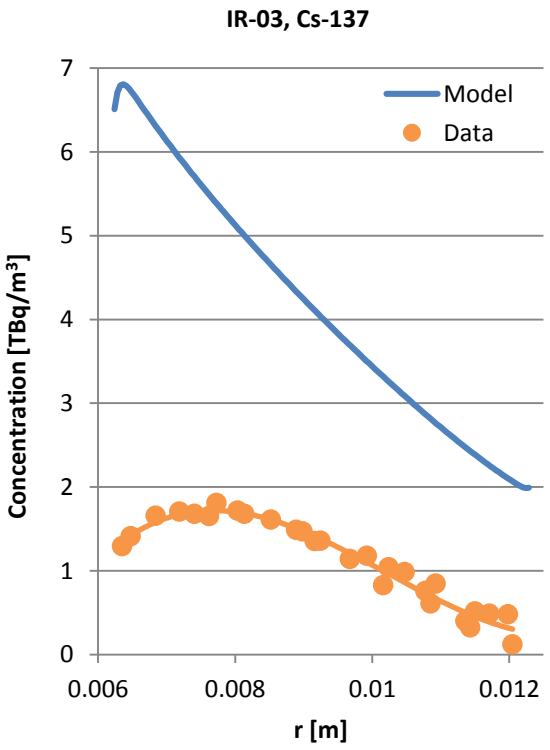

Fig. 12. Modeled vs. measured radial distribution of ^{137}Cs in the inner ring of capsule 3.

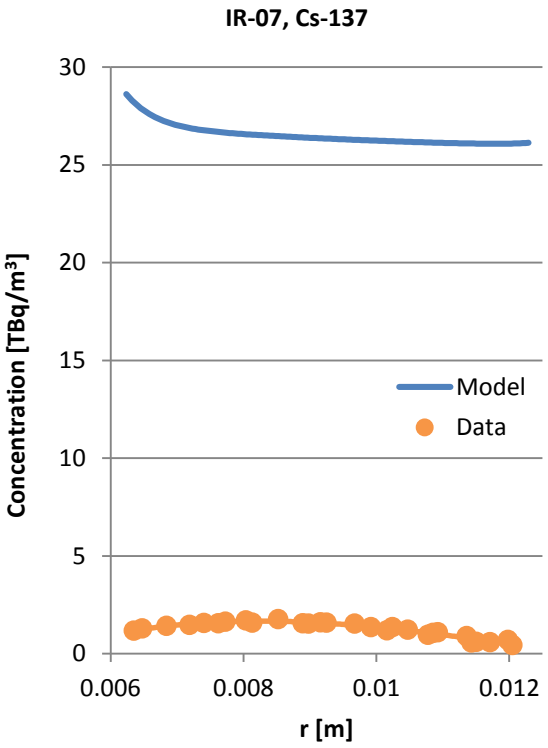

Fig. 13. Modeled vs. measured radial distribution of ^{137}Cs in the inner ring of capsule 7.

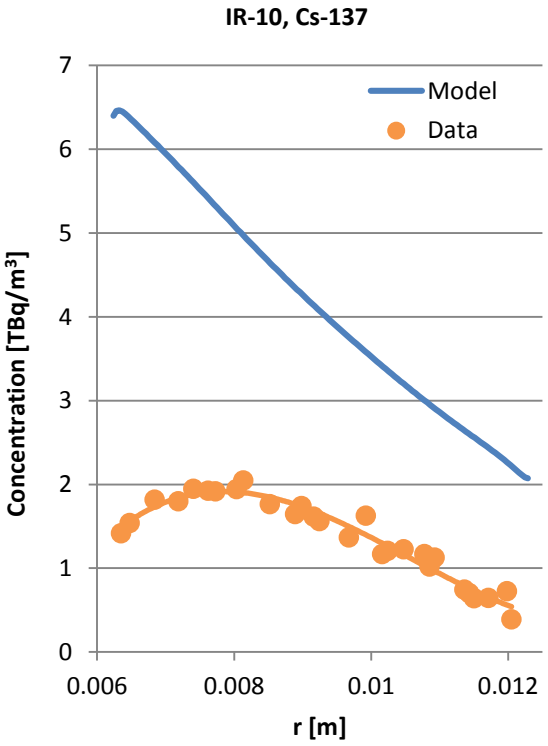

Fig. 14. Modeled vs. measured radial distribution of ^{137}Cs in the inner ring of capsule 10.

A noteworthy feature of the experimental profiles seen above is the peak in the curves toward the inner edge of the rings,* and decrease from there to the inner ring edge. This is not expected for a case where the temperature is monotonically decreasing with radius, which should result in similarly decreasing fission product concentrations moving outward across each ring. At this time it is not yet clear whether this measured trend is real, or a numerical artifact resulting from the inverse Radon transform employed in the tomography; some earlier numerical experiments with simulated profiles produced similar effects. This will become clear during PIE, when direct measurements of material sampled from the rings will be performed.

V. DETERMINING DIFFUSION COEFFICIENTS

We have described above a combination of computational models that, given a set of diffusion coefficients (among many other parameters), predict the resultant fission product concentration profiles in AGR-3/4. In actuality, our primary objective is to solve the inverse problem; fission product concentration profiles will be measured during post-irradiation examination, and we wish to infer from these the diffusion coefficients for the fission products and materials in question.

This task is complicated by several factors. First, there are a large number of parameters to solve for. Sixteen related to diffusion and sorption are required to model a single fission product in an AGR-3/4 capsule in the COMSOL model alone (see Tables III and IV); at least six more related to diffusion in PARFUME are the subject of active experimental investigation themselves. The number of unknowns, then, that one needs to determine to describe a profile is probably approaching the number of measurements that can be taken to define that profile. Finally, the nature of the modeling process, in which output from several codes is provided manually as input for a subsequent computation, is also not so amenable to any kind of direct numerical optimization.

We therefore seek some simplified approaches to obtaining diffusion coefficients from the measured data that minimize the influence of the other parameters. We describe some such methods in this section. Throughout, we use numerical experiments to test these approaches, using the model predictions described above as simulated data. The model takes diffusion coefficients as input and

* A qualitatively similar feature is evident in the model profiles in Figs. 12 and 14, which have a less pronounced peak nearer the inner edge of the ring. This, however, is a numerical artifact; the thermal analysis uses one day time steps, the last of which averages part of a full power day and part of a zero power day, resulting in an abrupt temperature drop and corresponding change in the boundary concentration given by the sorption isotherms.

produces fission product concentration profiles as output; a valid method of recovering these from the experiment data, applied to the model results, should recover, to a reasonable degree of accuracy, the diffusion coefficients used to produce them. We use this metric to judge the methods described below.

V.A. Standard Methods

Two commonly employed methods of measuring diffusion coefficients make use of steady-state and transient solutions, respectively, of the diffusion equation. In the latter case, we rely on an effectively infinite medium, and make an estimate based on the measured distance to which material has diffused during the course of the experiment. Based on the model calculations, neither case is particularly apt; most rings have built up some concentration of fission products across their entire width by the end of irradiation, but none have reached a truly steady state. Nevertheless, a steady state solution may be useful should it prove to give an approximately correct result, and we consider this possibility below.

V.A.1. Steady-state solution

For a cylindrical ring with fixed concentration C_1 at inner radius a, and likewise C_2 at outer radius b, the steady state concentration profile is given by

$$C(r) = C_1 + \frac{(C_2 - C_1)\ln\left(r/a\right)}{\ln\left(b/a\right)}. \qquad (5)$$

The radial flux J through the ring is therefore constant in time, and given by

$$J = \frac{D(C_1 - C_2)}{b\ln\left(b/a\right)} \qquad (6)$$

Integrating the above gives the total inventory M that has passed through the ring during time t. This is simply rearranged to give an expression for the diffusion coefficient D:

$$D = \frac{M\ln\left(b/a\right)}{2\pi Lt(C_1 - C_2)} \qquad (7)$$

Here L is the length of the ring. Geometric parameters a, b, and L, and irradiation time t, are known *a priori*; the inventory accumulated outside the ring (M) and the concentrations can be measured in PIE.

To test the method, we extract M, C_1, and C_2 from the model result for each capsule, and calculate D using Eq. 7. Using the TAVA temperatures for each ring (Table I), we can then construct an Arrhenius plot for this estimated diffusion coefficient, and compare it to the one that was actually input. An example is shown in Fig. 15 for Ag in matrix, which we know to have to the highest diffusion coefficient of the cases modeled and therefore expect to most closely approach steady state. It is clear from the figure, however, that the estimate is poor; it under-predicts the input diffusion coefficient by ~1-3 orders of magnitude over the experimental temperature range, a non-conservative result.

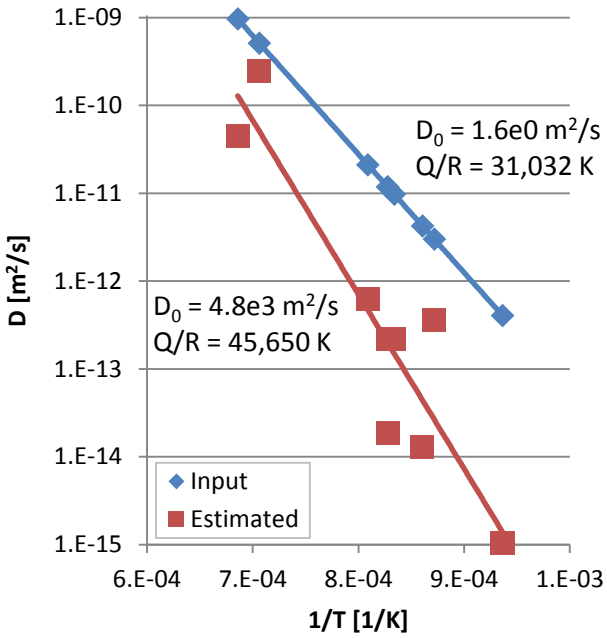

Fig. 15. Input diffusion coefficient for Ag in matrix vs. estimate based on a steady state assumption.

V.B. A more general analytical solution

It is clear based on the above example that a more general analytical description is needed to properly estimate the diffusion coefficient. To formulate one, first note that the transient solution to Eq. 1 for diffusion through a cylindrical annulus with fixed concentrations $C(a,t)=C_1$ and $C(b,t)=C_2$ at inner and outer radii a and b, respectively, has been given by Crank.[17] For an initial profile $C(r,0) = 0$, it is:

$$C(r,t) = \frac{C_1\ln\left(\frac{b}{r}\right) + C_2\ln\left(\frac{r}{a}\right)}{\ln\left(\frac{b}{a}\right)} - \pi\sum_{n=1}^{\infty}\frac{(C_2 J_0(a\alpha_n) - C_1 J_0(b\alpha_n))J_0(a\alpha_n)U_0(r\alpha_n)}{\exp\left(D\alpha_n^2 t\right)\left(J_0^2(a\alpha_n) - J_0^2(b\alpha_n)\right)} \qquad (8)$$

where

$$U_0(r\alpha_n) = J_0(r\alpha_n)Y_0(b\alpha_n) - J_0(b\alpha_n)Y_0(r\alpha_n) \qquad (9)$$

and α_n are the roots of

$$U_0(a\alpha_n) = 0 \qquad (10)$$

Secondly, we posit that the effect of complications such as sorption isotherms, time varying source terms, etc. can be captured in our estimation procedure by applying appropriate time-varying boundary conditions. In this case we can construct an analytical solution by applying Duhamel's theorem,[18]

$$C(r,t) = \int_0^t w(r,t-\tau)\frac{\partial f}{\partial \tau}\partial\tau + f(0)w(r,t) \qquad (11)$$

which gives the solution to Eq. 1 for *C(a,t)=f(t)*, *C(b,t)=0*, and *C(r,0)=0* where *w(r,t)* is the fundamental solution to the same equation with *w(a,t)=1*, *w(b,t)=0*, and *w(r,0)=0*. The latter is clearly given by Eq. 8 with $C_1=1$ and $C_2=0$. Following Ref. 19, we can account for time-varying boundary conditions at both *a* and *b* by solving two sub-problems, each with a single inhomogeneity, and superposing their solutions, i.e.

$$C(r,t) = C_f(r,t) + C_g(r,t) \qquad (12)$$

Based on the above boundary conditions, we have

$$w_f(r,t) = \frac{\ln\left(\frac{b}{r}\right)}{\ln\left(\frac{b}{a}\right)} + \pi\sum_{n=1}^{\infty}\frac{J_0(b\alpha_n)J_0(a\alpha_n)U_0(r\alpha_n)}{\exp\left(D\alpha_n^2 t\right)\left(J_0^2(a\alpha_n) - J_0^2(b\alpha_n)\right)} \qquad (13)$$

and

$$C_f(r,t) = f(t)\frac{\ln\left(\frac{b}{r}\right)}{\ln\left(\frac{b}{a}\right)} + \pi\sum_{n=1}^{\infty}\left[\frac{J_0(b\alpha_n)J_0(a\alpha_n)U_0(r\alpha_n)}{\exp\left(D\alpha_n^2 t\right)\left(J_0^2(a\alpha_n) - J_0^2(b\alpha_n)\right)} \times\left(f(0) + \int_0^t f'(\tau)\exp\left(D\alpha_n^2\tau\right)d\tau\right)\right] \qquad (14)$$

Likewise for $C_g(a,t)=0$, $C_g(b,t)=g(t)$, $C_g(r,0)=0$ and $w_g(a,t)=0$, $w_g(b,t)=1$, and $w_g(r,0)=0$,

$$w_g(r,t) = \frac{\ln\left(\frac{r}{a}\right)}{\ln\left(\frac{b}{a}\right)} - \pi\sum_{n=1}^{\infty}\frac{\exp\left(-D\alpha_n^2 t\right)J_0^2(a\alpha_n)U_0(r\alpha_n)}{\left(J_0^2(a\alpha_n) - J_0^2(b\alpha_n)\right)} \qquad (15)$$

and

$$C_g(r,t) = g(t)\frac{\ln\left(\frac{r}{a}\right)}{\ln\left(\frac{b}{a}\right)} - \pi\sum_{n=1}^{\infty}\left[\frac{\exp\left(-D\alpha_n^2 t\right)J_0^2(a\alpha_n)U_0(r\alpha_n)}{\left(J_0^2(a\alpha_n) - J_0^2(b\alpha_n)\right)} \times\left(g(0) + \int_0^t g'(\tau)\exp\left(D\alpha_n^2\tau\right)d\tau\right)\right] \qquad (16)$$

And therefore the general solution for *C(a,t)=f(t)*, *C(b,t)=g(t)*, and *C(r,0)=0* is given by†

$$C(r,t) = \frac{f(t)\ln\left(\frac{b}{r}\right) + g(t)\ln\left(\frac{r}{a}\right)}{\ln\left(\frac{b}{a}\right)} - \pi\sum_{n=1}^{\infty}\left\{\frac{J_0(b\alpha_n)J_0(a\alpha_n)U_0(r\alpha_n)}{\exp\left(D\alpha_n^2 t\right)\left(J_0^2(a\alpha_n) - J_0^2(b\alpha_n)\right)} \times\left[J_0(a\alpha_n)\left(g(0) + \int_0^t g'(\tau)\exp\left(D\alpha_n^2\tau\right)d\tau\right) - J_0(b\alpha_n)\left(f(0) + \int_0^t f'(\tau)\exp\left(D\alpha_n^2\tau\right)d\tau\right)\right]\right\} \qquad (17)$$

Here the actual form of the time-dependent boundary conditions is left unspecified; in what follows, we use polynomials, in which case the integrals in Eq. 17 can be evaluated analytically.

To test the applicability of this solution, we conduct a numerical experiment as before, and have written a

† In the numbering system for heat conduction problems proposed in Ref. 20 and elaborated upon in Ref. 21, this represents the solution to the R11B--T0 problem.

program in R (Ref. 22) to do so. First, the model predictions of the time-varying boundary concentrations are fitted with polynomials (of any desired order). Using these fit functions for the boundary conditions *f(t)* and *g(t)*, we then fit Eq. 17‡ to the profile predicted by the model, using a non-linear least squares method to estimate *D*. In this case, we find that the estimated *D* is close to the input value, less than a factor of two different for Ag and Cs, in capsule three. The results of these numerical experiments are summarized in Table VII.

TABLE VII. Comparison of model input diffusion coefficients and values estimated by fitting Eq. 17 to capsule 3 results.

		Input D (m^2/s)	Estimate‡ D (m^2/s)	Within factor of:	Quasi-Steady?
Ag	IR	5.56e-12	9.11e-12	1.64	Yes
	OR	2.68e-12	3.36e-12	1.25	Yes
Cs	IR	1.39e-12	1.09e-12	1.27	Yes
	OR	6.72e-13	1.06e-12	1.58	No
Sr	IR	1.23e-13	3.51e-13	2.85	No
	OR	5.17e-14	1.12e-13	2.17	No

‡This varies in time and space as the temperatures change; we use here the time-averaged boundary temperature that maximizes the difference between input and estimate.

The input and estimated values for *D* cannot match exactly, as the polynomial description of the boundary conditions is necessarily inexact. Figs. 16-17 show some examples of the boundary concentrations predicted by the model, and the polynomial fits. Resulting as they do from as-run temperature predictions and calculations of release from particles that depend on them in turn, the predicted values are somewhat chaotic due to the changing conditions during irradiation, especially periodic shutdowns. They are nevertheless reasonably described by polynomials, and the success of the numerical experiment demonstrates this.

Figs. 18-19 demonstrate the range of regimes occurring in the model. Fig. 18 shows a case that is quasi-steady, i.e. the solution is approximately steady-state based on the boundary values at a given time; here the exponential terms in Eq. 17 have decayed away, and the solution is well approximated by the first term. Note that the flux still varies in time, and depends on the boundary condition functions. Fig. 19 shows a case that is still far from steady state; no concentration has built up at the outer boundary, and all terms of Eq. 17 are necessary to describe this case. The fit including all terms of Eq. 17, which describes the model profile well, is shown alongside the quasi-steady form (the first term of Eq. 17 only) to illustrate the difference.

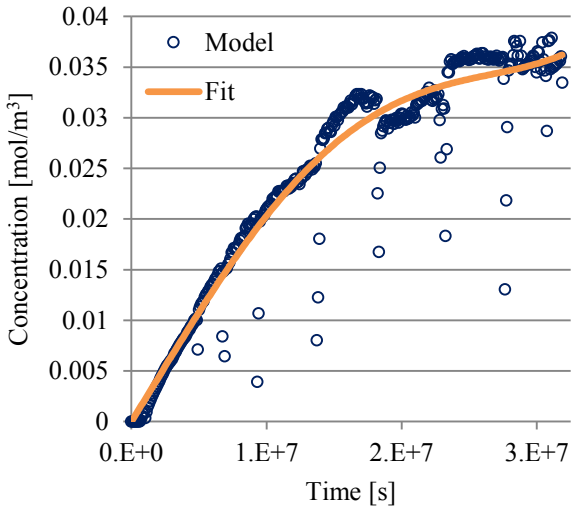

Fig. 16. Cs concentration at the inner boundary of IR-03 as a function of time: model prediction and polynomial fit.

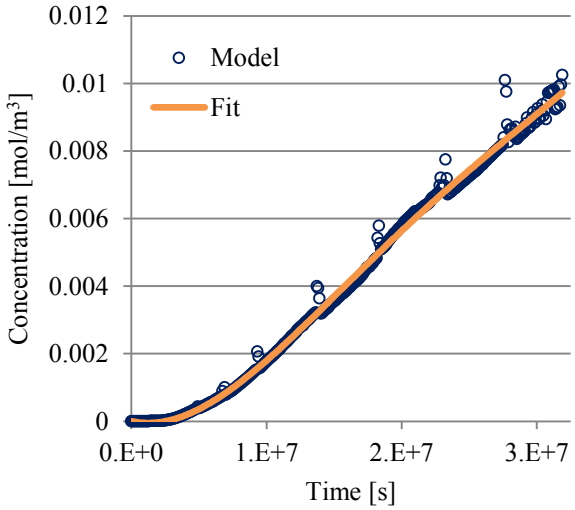

Fig. 17. Cs concentration at the outer boundary of IR-03 as a function of time: model prediction and polynomial fit.

Thus, Eq. 17 appears to describe well the fission product diffusion behavior anticipated in AGR-3/4, with the combined effects of temperature-dependent release from particles and sorption isotherms described by time-varying polynomial boundary conditions. In applying it to fit measured data, however, we cannot in fact know how these boundary concentrations changed over time—only the final value. The fits to model predictions (scaled to match the measured final value if necessary) can be used initially, but in the event the determined value of *D*

‡Our fitting procedure takes as input the desired accuracy, and computes the required number of terms to sum to achieve it, as described in Ref. 23. We have also adapted the method described in that work for computing the roots α_n of Eq. 10.

differs significantly from that used to generate the boundary conditions via the model, some iteration will be necessary here.

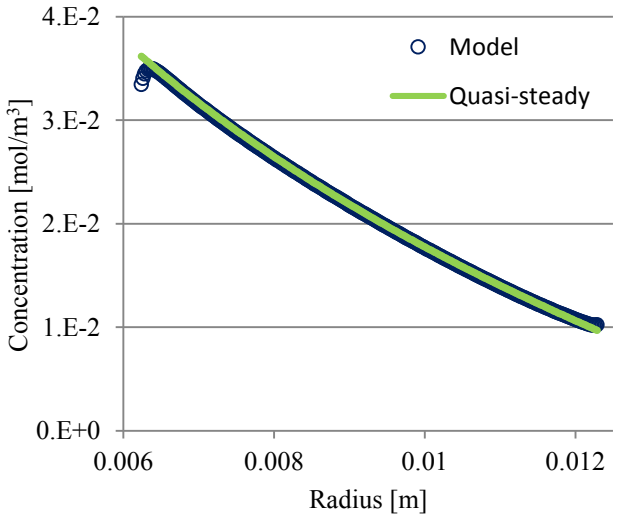

Fig. 18. Cs radial profile across IR-03: model prediction and fit using the first term in Eq. 17. This case is quasi-steady.

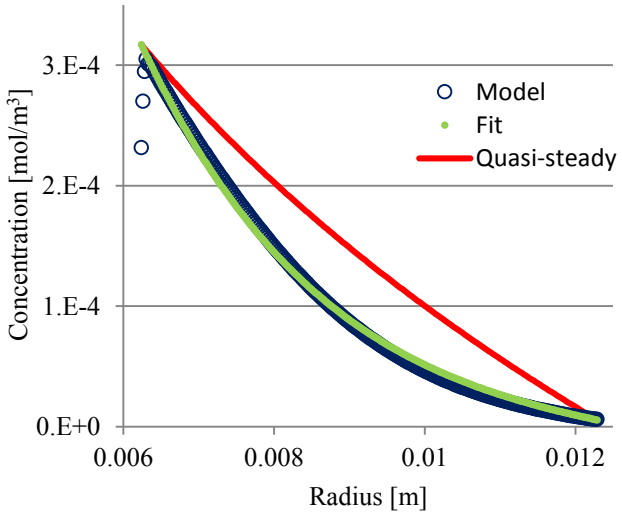

Fig. 19. Sr radial profile across IR-03: model prediction and fit using Eq. 17. Little Sr has diffused into this ring, and the outer boundary remains ~0.

V.C. An estimate of the diffusion coefficient in Europium

Our efforts to model Ag, Cs, and Sr transport based on diffusion coefficient data in the existing literature have been outlined above. Another isotope of interest is ^{154}Eu, which was generally not detected in the gamma scanning, but for which a clear profile was measured in the inner ring of capsule 7, which was the hottest capsule in the experiment. Using the analytical method described in the preceding section, we make a first estimate of the europium diffusion coefficient here.

As noted above, we cannot know from post-irradiation measurements how the concentration varied as a function of time. Neither do we have an estimate of the diffusion coefficient for europium, even from legacy data. We know only the final concentration, and that it was initially zero. The simplest valid assumption satisfying these constraints is a linear increase in time from zero to the final measured value. As europium is thought to have similar transport properties to strontium, we can additionally consult the model prediction for strontium in the inner ring of capsule 7, which is shown in Fig. 20. This, too, is relatively linear. So, we adopt a linear function for $f(t)$, adjusting the slope to match the measured final value. The resultant fit is shown alongside the data (azimuthally averaged as described in Sec. IV) in Fig. 21. It gives D=1.17e-13 m^2/s, and this value is plotted at the TAVA temperature for IR-07 (1151 °C) and compared to the existing diffusion coefficients for Ag, Cs, and Sr in Fig. 22, where it is clear that this value is indeed very close to that for strontium in matrix. This estimate will continue to be refined as data are collected during AGR-3/4 PIE.

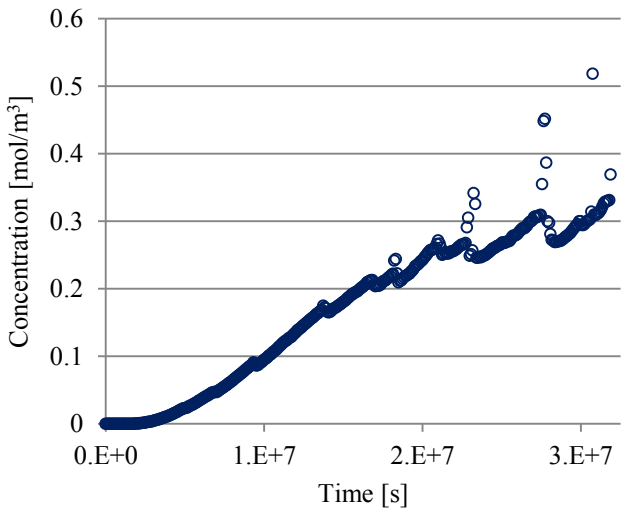

Fig. 20. Model prediction of the Sr concentration at the inner boundary of IR-07 as a function of time.

VI. CONCLUSIONS AND FUTURE WORK

We have described here an established methodology for modeling fission product transport in HTGRs, and its application to the AGR-3/4 experiment. Preliminary comparisons to fission product concentration profiles measured by gamma scanning indicate reasonable (+/- one order of magnitude) agreement in many cases using legacy diffusion coefficient and sorption isotherm data.

Our ultimate objective being to refine estimates of these parameters based on AGR-3/4 data, we have identified an analytical method for doing so that partially eliminates the complexity resulting from temporally and spatially varying temperatures and source terms by describing these simply with time-varying boundary conditions. A series of numerical experiments was conducted which successfully verified that the technique is reasonably accurate (within a factor of 2-3), though some insight from the model is still required to ascertain the proper form of these boundary conditions. In analyzing the experiment data, some iteration between the analysis and the model will be necessary to ensure consistency.

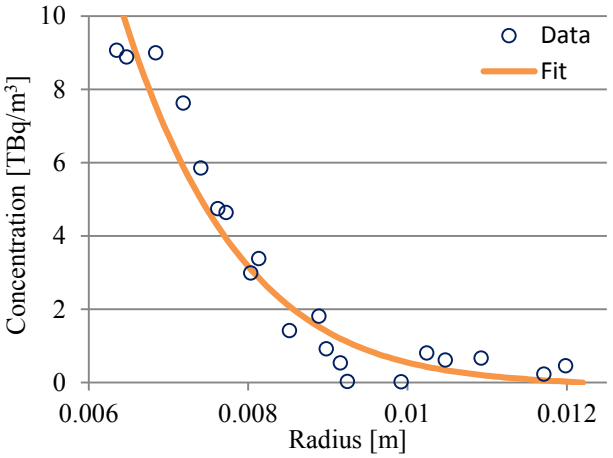

Fig. 21. Measured ^{154}Eu radial profile across IR-07 and Eq. 17 fit giving D=1.17e-13 m^2/s.

We are still in the process of laying out a specific PIE plan for AGR-3/4, and the model is aiding in this effort. In addition to the originally-planned destructive analysis and safety tests, an additional contingency is being considered. Should fission product profiles measured by destructive sampling prove difficult to analyze (e.g. if multiple or no sets of diffusion coefficients can be found that consistently describe data from multiple capsules), some of rings may be used instead for a separate effects test in which they are isolated and heated at constant temperature so as to measure only a single parameter, the diffusion coefficient, based on the change in concentration profile. We are in the process of simulating such tests using the model, to identify the anticipated duration of the tests necessary to sufficiently modify the initial fission product profiles without releasing the entire inventory. Accurate determination of the initial profile in the absence of a destructive measurement may be another challenge in conducting these tests, and sensitivity studies are planned to further explore this.

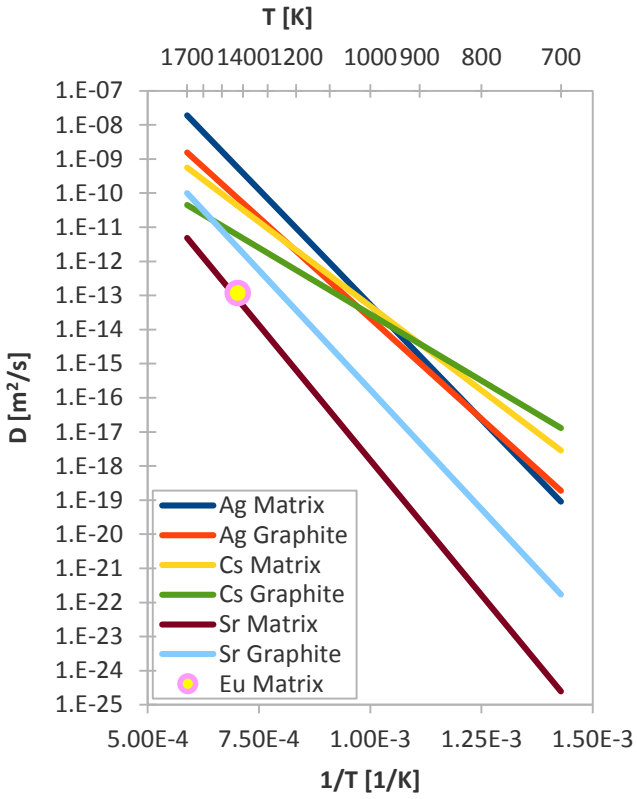

Fig. 22. Diffusion coefficient for europium in matrix compared to Ag, Cs, and Sr.

REFERENCES

1. *Technical Program Plan for INL Advanced Reactor Technologies Technology Development Office/Advanced Gas Reactor Fuel Development and Qualification Program*, PLN-3636 rev. 5, Idaho National Laboratory (2016).
2. J. M. HARP, P.A. DEMKOWICZ, J.D. STEMPIEN, "Initial gamma spectrometry examination of the AGR-3/4 irradiation," *Proceedings of HTR2016*, Las Vegas, Nevada, USA, November 6–10, 2016, Paper 18594.
3. B. P. COLLIN and P. W. HUMRICKHOUSE, *AGR-3/4 Irradiation Experiment Test Plan*, PLN-3867 rev. 1, Idaho National Laboratory (2015).
4. S. B. GROVER and D. A. PETTI, "Design and status of the NGNP fuel experiment AGR-3/4 irradiated in the advanced test reactor," *Nuclear Engineering and Design*, **271**, 142–148 (2014).
5. B. P. COLLIN, *AGR-3/4 Irradiation Test Final As-Run Report*, INL/EXT-15-35550 rev. 1 (2016).
6. G. L. HAWKES, "AGR-3/4 Daily As-Run Thermal Analysis," ECAR-2807 rev. 1, Idaho National Laboratory (2016).

7. J. W. STERBENTZ, "JMOCUP As-Run Daily Physics Depletion Calculation for the AGR-3/4 TRISO Particle Experiment in ATR Northeast Flux Trap," ECAR-2753, Idaho National Laboratory (2015).
8. G. L. HAWKES et al., "Thermal predictions of the AGR-3/4 experiment using PIE-measured time varying gas gaps," *Proceedings of the ASME 2016 International Mechanical Engineering Congress and Exposition (IMECE2016)*, Phoenix, AZ, November 11–17 2016, ASME (2016).
9. W. F. SKERJANC, *AGR-3/4 Irradiation Test Predictions using PARFUME*, INL/EXT-16-38280 (2016).
10. B. P. COLLIN et al., "Comparison of silver, cesium, and strontium release predictions using PARFUME with results from the AGR-1 irradiation experiment," *Journal of Nuclear Materials*, **466**, 426–442 (2015).
11. B. P. COLLIN et al., "Comparison of fission product release predictions using PARFUME with results from the AGR-1 safety tests," *Nuclear Engineering and Design*, **301**, 378–390 (2016).
12. J. CROZIER, *Fission Product Transport Predictions forAGR-3/4*, General Atomics report 911200 (2011).
13. B. F. MYERS, *Fuel Design Data Manual*, General Atomics report 901866 Issue F (1987).
14. *Fuel Performance and Fission Product Behavior in Gas Cooled Reactors*, IAEA TECDOC-978 (1997).
15. B. F. MYERS and W. E. BELL, *Strontium transport data for HTGR systems*, General Atomics report GA-A13168 (1974).
16. R. C. MARTIN, *Compilation of Fuel Performance and Fission Product Transport Models and Database for MHTGR Design*, ORNL/NPR-91/6 (1993).
17. J. CRANK, *The Mathematics of Diffusion*, pp. 84, 2nd Ed., Clarendon Press, Oxford, UK (1975).
18. S. J. FARLOW, *Partial Differential Equations for Scientists and Engineers*, pp. 106–111, Dover Publications Inc., New York, NY (1993).
19. G. E. MYERS, *Analytical Methods in Conduction Heat Transfer*, pp. 141–148, 2nd Ed., AMCHT Publications, Madison, WI (1998).
20. J. V. BECK and B. LITKOUHI, "Heat conduction number system," *International Journal of Heat and Mass Transfer*, **31**, 505–515 (1988).
21. K. D. COLE et al., *Heat Conduction Using Green's Functions*, pp. 47–62, 2nd Ed., Taylor and Francis, Boca Raton, FL (2011).
22. *R: A Language and Environment for Statistical Computing*, R Foundation for Statistical Computing, Vienna, Austria, http://www.R-project.org (2016).
23. S. NALLAPANENI and J. V. BECK, "Hollow Cylinder, temperature jump at inner boundary and zero temperature at outer boundary," *ExACT Analytical Conduction Toolbox*, http://exact.unl.edu (2014).